RESEARCH ARTICLE
SPACE PHYSICS

Earth and Planetary Physics
10: 136–143, 2026
doi: 10.26464/epp2026008

Case studies of ion focusing in the downstream region of a modeled low Earth orbit spacecraft

Nizam Ahmad[1*], Hideyuki Usui[2], Yohei Miyake[2], Slamet Supriadi[1], Hanif Fakhrurroja[1,3*], Hilman Syaeful Alam[1], and Harry Bangkit[1]

[1]Research Center for Smart Mechatronics, National Research and Innovation Agency, 40135 Bandung, Indonesia;

[2]Graduate School of System Informatics, Kobe University, Kobe, Japan;

[3]School of Industrial Engineering, Telkom University, 40257 Bandung, Indonesia

Key Points:

- Ion-focusing formations behind spacecraft in low orbit are due to electric fields and are not significantly influenced by geophysical changes.
- Higher plasma density increases the ion concentration locally but does not shift the overall ion-focusing structure.
- The spacecraft potential strongly distorts the ion void and enhances ion focusing in the downstream region.

Citation: Ahmad, N., Usui, H., Miyake, Y., Supriadi, S., Fakhrurroja, H., Alam, H. S., and Bangkit, H. (2026). Case studies of ion focusing in the downstream region of a modeled low Earth orbit spacecraft. *Earth Planet. Phys.*, *10*(1), 136–143. http://doi.org/10.26464/epp2026008

Abstract: The effect of plasma and charged particle interaction with spacecraft in a low Earth orbit (LEO) environment leads to ion focusing and the formation of an ion void in the downstream region as a result of charging. Simulations and investigations using a fixed potential imposed on the spacecraft showed the nonsignificance of geophysical parameter changes to ion focusing. Variation of the temperature ratio (T_r) contributed only to local ion focusing and manifested as two-ion streamers dispersed at the upper and lower edges of the spacecraft—the outermost layers of the satellite structure at the top and bottom, respectively. A simulation involving changing the ambient plasma density (N_p) also showed the formation of local ion focusing, in which ions were more concentrated as the density increased. Furthermore, auroral electron density (N_{ae}) variation had no clear impact on ion focusing, as indicated by static two-ion structures in the wake field. However, variation of the object potential (ϕ) strongly affected ion focusing formation, leading to distortion of the initial ion void region behind the spacecraft. The formation of ion focusing in this study was subject to the electric field produced by the object potential and the ambipolar electric field resulting from plasma expansion in the downstream region.

Keywords: ion focusing; spacecraft potential; low Earth orbit environment

1. Introduction

It is a fact that the need for satellite industries is growing rapidly and that satellites are being used for multiple purposes. The current number of orbiting satellites is approximately 1700, distributed at three altitudes: low Earth orbit (LEO: 200–1000 km), medium Earth orbit (MEO: 10,000–20,000 km), and geostationary Earth orbit (GEO: 36,000 km). The launch of a satellite into space, including its maintenance, is of great concern because of the high-cost technology, so substantial efforts are needed alongside its operation to mitigate the risk of failure.

Because the space environment leads to multiple effects when interacting with satellites, the knowledge of how space plasma and electromagnetic radiation affect the object in space becomes a primary concern in the field of spacecraft charging (Garrett and Whittlesey, 2000), given that spacecraft charging is believed to be the main trigger of spacecraft failures or anomalies in space (Koons et al., 2000). In addition, spacecraft failures in the LEO environment are mostly subject to precipitated auroral electron fluxes during geomagnetically disturbed conditions (Ahmad et al., 2018a), leading to various effects from low-level to severe charging. The impact of auroral electrons on spacecraft charging has been simulated by using Electro-Magnetic Spacecraft Environment Simulator (EMSES) particle-in-cell (PIC) software (e.g., Ahmad et al., 2018b).

The charging of spacecraft is significantly influenced by the equilibrium of plasma inflow or outflow present (Katz et al., 1987). If the spacecraft experiences a greater influx of incoming currents compared with departing currents, the potential difference across the spacecraft will first rise and then decrease until equilibrium in the net current is achieved (Hastings, 1995). In several instances, electron currents contribute substantially to the charging process. Because of the disparity in thermal equilibrium mass between electrons and protons, electrons exhibit much greater velocities than protons (approximately 43 times more; Baumjohann and

Correspondence to: N. Ahmad, nizam.ahmad@brin.go.id
H. Fakhrurroja, haniff@telkomuniversity.ac.id
Received 25 APR 2024; Accepted 16 SEP 2025.
First Published online 30 SEP 2025.

Treumann, 1997). This disparity leads to a more pronounced effect of electron currents on spacecraft than ion currents. This may be seen as a rise in the negative voltage of the spacecraft resulting from incoming electron currents, contingent on the plasma density and the spacecraft potential (Frooninckx and Sojka, 1992).

Although spacecraft charging in the LEO environment is an important issue, this study highlights the importance of investigating plasma behaviors on the downstream side of the spacecraft—specifically, the formation of ion-rich regions, or ion focusing. These regions are crucial because they can substantially influence the local plasma–satellite interactions, potentially affecting surface charging, sensor readings, and even material degradation over time. Having an understanding of these downstream behaviors can help designers create more robust spacecraft systems and increase the accuracy of models of plasma interactions by providing important information about the space environment surrounding the spacecraft. Within these regions, the ambient plasma motion near the spacecraft is observed to exhibit mesothermal characteristics, assuming the thermal conditions are maintained (Hastings and Garrett, 1996). The ions flow supersonically, whereas the electrons move subsonically, and the inequality condition is satisfied ($V_{\mathrm{th_i}} < V_{\mathrm{sc}} < V_{\mathrm{th_e}}$). The thermal speed is calculated through the following equation:

$$V_{\mathrm{th_{e,i}}} = \sqrt{\frac{2kT_{\mathrm{e,i}}}{m_{\mathrm{e,i}}}},$$

where k designates the Boltzmann constant (J/K), T is temperature (K), m is particle mass (kg), and the subscripts e and i represent the electron and ion species, respectively. Here, $V_{\mathrm{th_i}}$ and $V_{\mathrm{th_e}}$ refer to the thermal speed of ions and electrons, respectively, whereas V_{sc} denotes the spacecraft orbital speed. Fulfilling the aforementioned condition results in wake formation behind the spacecraft from which the ion void region is formed (e.g., Ahmad et al., 2019; Ahmad and Usui, 2020). The presence of a plasma wake has been demonstrated through laboratory experiments using a biased plate, showing that ion flows are strongly affected by the potential imposed on the plate (Katz et al., 1986). The plasma wake has also been shown through *in situ* observations around an S-520-26 ionospheric sounding rocket, revealing localized hot plasmas surrounding the wake structure that could cause a variety of plasma instabilities (Endo et al., 2015). Inside the wake region, electron and ion densities decline intrusively toward the wake centerline. However, the electron density significantly exceeds that of ions, with an overall rate of 50% observed in this study.

Under some circumstances, the ion void area can vanish and transform into ion focusing. In this case, ion focusing is formed as a result of the merging of two-ion streamers that flow from the upper and lower edges of the spacecraft and converge behind it. In this situation, the ion density rapidly escalates to a distance of several Debye lengths behind the object. The strength of ion focusing rises with the rising temperature ratio between electrons and ions (e.g., Okada et al., 1995; Miloch, 2010). The path of ambient plasma, particularly ions, is altered by a much more intense electric field near the sheath boundary of the spacecraft.

A question emerges over whether the temperature ratio of electrons to ions ($T_{\mathrm{r}} = T_{\mathrm{e}}/T_{\mathrm{i}}$) is the primary determinant of the ion-concentrating zone behind the spacecraft or whether other characteristics must also be considered. Consequently, we wished to analyze various environmental characteristics within a specific set of simulations to determine which factors effectively contribute to ion concentration in the downstream area.

2. Data and Methods

To obtain intricate characteristics of the ambient plasma distribution around the spacecraft, we conduct numerical simulations using the program EMSES, based on the PIC method (Miyake and Usui, 2009). The EMSES software analyzes electrostatic phenomena in space plasma and the spacecraft surface potential. A spacecraft is assumed to be a perfect conductor immersed in plasma, and particles impinge on the surface of the spacecraft in a self-consistent manner. These particles are absorbed, and their charges build on the surface of the spacecraft. The floating potential of the spacecraft is achieved when the net current at its surface equals zero.

The width of the spatial grid (Δr) in a simulation domain is set as smaller than the Debye length (λ_{D}) for the stability of the simulation; therefore, Δr = 0.5 cm is used in all simulations. To satisfy the condition λ_{D} > 5.5 cm, the plasma environment parameters are chosen such that the electron temperature (T_{e}) ranges from 3000 to 5000 K and the ambient plasma density (N_{p}) is between 10^9 and 10^{10} m^{-3}. These values reflect the typical density of the ionospheric plasma in the LEO regime. The grid dimensions for each axis (N_x, N_y, N_z) are 256, resulting in a simulation box volume of 128^3 cm^3. The ion-to-electron mass ratio should closely approximate the actual value to accurately represent the density distribution around the spacecraft, particularly in the downstream area. It is challenging to replicate the actual geometry of the LEO spacecraft in terms of both shape and size. Thus, for computational efficiency, we scaled the modeled structure so that 1 cm in the simulation domain would represent 1 m in actual dimensions. We used a simple box-shaped model with dimensions of 6 × 6 × 12 cm. This choice was made after a series of tests aimed at avoiding time-consuming simulations and visualizing plasma features clearly, particularly on the sheath edges of the spacecraft. In addition, we used this geometry for two reasons: (1) its dimensions were limited because the EMSES tool commonly simulates two types of shapes, rectangular and cylindrical bodies, and (2) most failures on LEO satellites in our previous study (Ahmad et al., 2018b) were box-shaped, so simulating the effect of particle interaction on part of the satellite structure is expected to provide an overview of plasma behavior after interaction has occurred. Moreover, we set the position of the body at the middle of the simulation box domain; the simulation time step (Δt) is 10^2 ps per cycle (iteration), and the total number of time steps is 10^5. The simulation domain is established as shown in Figure 1.

As shown in Figure 1, plasma is assumed to flow in the opposite direction to spacecraft motion, which is in the +x direction, whereas precipitated auroral electrons flow in the opposite direction to the background magnetic field, which is in the –z direction (the spacecraft rest frame). Both plasma and auroral electrons are assumed to have a Maxwellian distribution with no collisions among particles. The effect of the geomagnetic field is omitted for

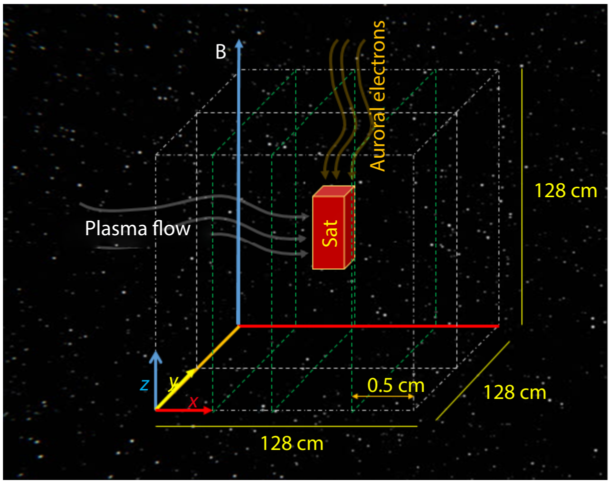

Figure 1. A simulation domain of interaction between a spacecraft (sat), ambient plasma, and auroral electrons (the spacecraft rest frame).

ion motion because the thermal ion Larmor radius (R_i) is larger than the spacecraft dimension (L) and thus larger than the magnetization parameter ($M \sim R_j/L$), where subscript j represents much smaller ($M \ll 1$) species of electrons (e) and ions (i). In contrast, because of its smaller Larmor radius (R_e), the electron motion is assumed to be magnetized ($M \gg 1$). The effect of the magnetic field on plasma (magnetized or unmagnetized) plays a role in estimating the density distribution around the spacecraft, especially in the downstream region (Engwall et al., 2006).

In this study, we initially simulate three cases, cases 1, 2, and 3, with electron-to-ion temperature ratios of 5, 2, and 1.1, respectively, as detailed in Table 1. In the LEO environment, because the temperature of electrons is higher than that of ions, the simulations set the ratio of the two temperatures at greater than 1. This step ensures that the electron temperature remains higher than the ion temperature. The temperature values for electrons and ions were derived from the International Reference Ionosphere (IRI) database, available at https://kauai.ccmc.gsfc.nasa.gov/instantrun/iri/. Note that in this simulation, achieving a floating potential of approximately −10 V requires a total of 2.10^6 iterations, which is a time-intensive process. To circumvent time-consuming simulations, we apply a fixed potential of −5, −10, −15, and −20 V to each case. The simulation (not presented in this article) indicated that the charging levels in the case of the floating potential are consistent with the these values. Note also that the use of the floating potential provides more realistic spacecraft charging conditions, particularly when auroral electrons are present. However, in the present study, we choose a fixed potential to expedite simulations and allow for parameter changes without compromising the validity of the results. The present simulations show that the floating potential results are well represented by the specified fixed potentials. In the case of the fixed potentials, we set the average thermal speed for electrons, ions, and auroral electrons as approximately 353, 5.8, and 5.5×10^4 km/s, respectively. The density of auroral electrons (N_{ae}) is maintained at a constant value of $10^6/m^3$ in each case. The ambient plasma density varies across cases, encompassing the lower to higher flux ratios of precipitated auroral electrons to ambient plasma (N_p), as shown in Table 1.

As Table 1 indicates, the notation T_r denotes the temperature ratio of plasma electrons (T_e) to plasma ions (T_i). We use the hydrogen ion H^+, or proton, for the present simulation. In this study, we initially conduct simulations utilizing the parameters outlined in Table 1. Note that ambient electron current densities are substan-

Table 1. Parameters used for spacecraft and plasma interactions in the LEO environment.

Case		T_e	T_i	T_r (T_e/T_i)	N_p (per m^3)	N_{ae} (per m^3)	Potential (V)
1		3750	750	5	10^9	10^6	−5, −10, −15, −20
2		4000	2000	2	10^8	10^6	−5, −10, −15, −20
3		4500	4050	1.1	10^7	10^6	−5, −10, −15, −20
4	a	3750	2000	1.9	10^8	10^6	−5
	b	4000	2000	2	10^8	10^6	−5
	c	4500	2000	2.3	10^8	10^6	−5
5	a	4000	1250	3.2	10^8	10^6	−5
	b	4000	2000	2	10^8	10^6	−5
	c	4000	2750	1.5	10^8	10^6	−5
6	a	4000	2000	2	10^9	10^6	−5
	b	4000	2000	2	10^8	10^6	−5
	c	4000	2000	2	10^7	10^6	−5
7	a	4000	2000	2	10^8	10^5	−5
	b	4000	2000	2	10^8	10^6	−5
	c	4000	2000	2	10^8	10^7	−5
	d	4000	2000	2	10^8	10^8	−5

tially higher than photoelectron current densities in the LEO regime; therefore, the latter can be disregarded (Hastings, 1995). To identify the parameter that significantly influences ion focusing, we conduct additional simulations in which one parameter is varied while the others are held constant. The subsequent section presents details of these simulations.

3. Results and Discussion

3.1 Fixed Potential with Varied Parameters

Formation of the ion-rich region for cases 1–3 is presented according to the parameters outlined in Table 1. The simulation results indicate that, in most cases, electrons are repelled from the spacecraft because of the negative potential. An increase in the spacecraft potential is observed to follow from a greater expulsion of electrons from the spacecraft. The absence of boundary effects on electron distribution is confirmed because the quasi-neutrality state is attained at the edges of the simulation box. The segregation of ambient electrons from the object results in an increased density of ambient ions, particularly on the downstream side of the spacecraft, as depicted in Figure 2. This section presents examples of ion density variations in case 1 across potentials ranging from −5 to −20 V.

Figure 2 illustrates the spacecraft as a red square positioned centrally within the simulation box domain, specifically between 122 and 134 cm on the *x*-axis. Here, we display the cross-section in the *x*–*z* plane and cut the plane along the *y*-axis at the center of the simulation box at the grid *y* = 128 cm. The ion density in the color bar is the normalized value obtained by comparing the ion density values after interaction with the initial plasma density values before interacting with the spacecraft. We can see from Figure 2 that the ion-focusing regions exhibit variations in all cases. The reduction in negative potential of the object results in a distinct ion-focusing region. At a potential of −5 V, the ion-rich region divides into two triangular structures, as illustrated in Figure 2a. The two initially separated structures commence merging toward the wake centerline, resulting in the compression of the initial ion void structure, as illustrated in Figure 2b. As the potential decreases, the distortion of the ion void structure intensifies, resulting in a greater attraction of ions to the object, as illustrated in Figure 2c. An ion-focusing region is established, characterized by the gradual disappearance of the ion void structure, as illustrated in Figure 2d. Figure 2 illustrates that the length of the

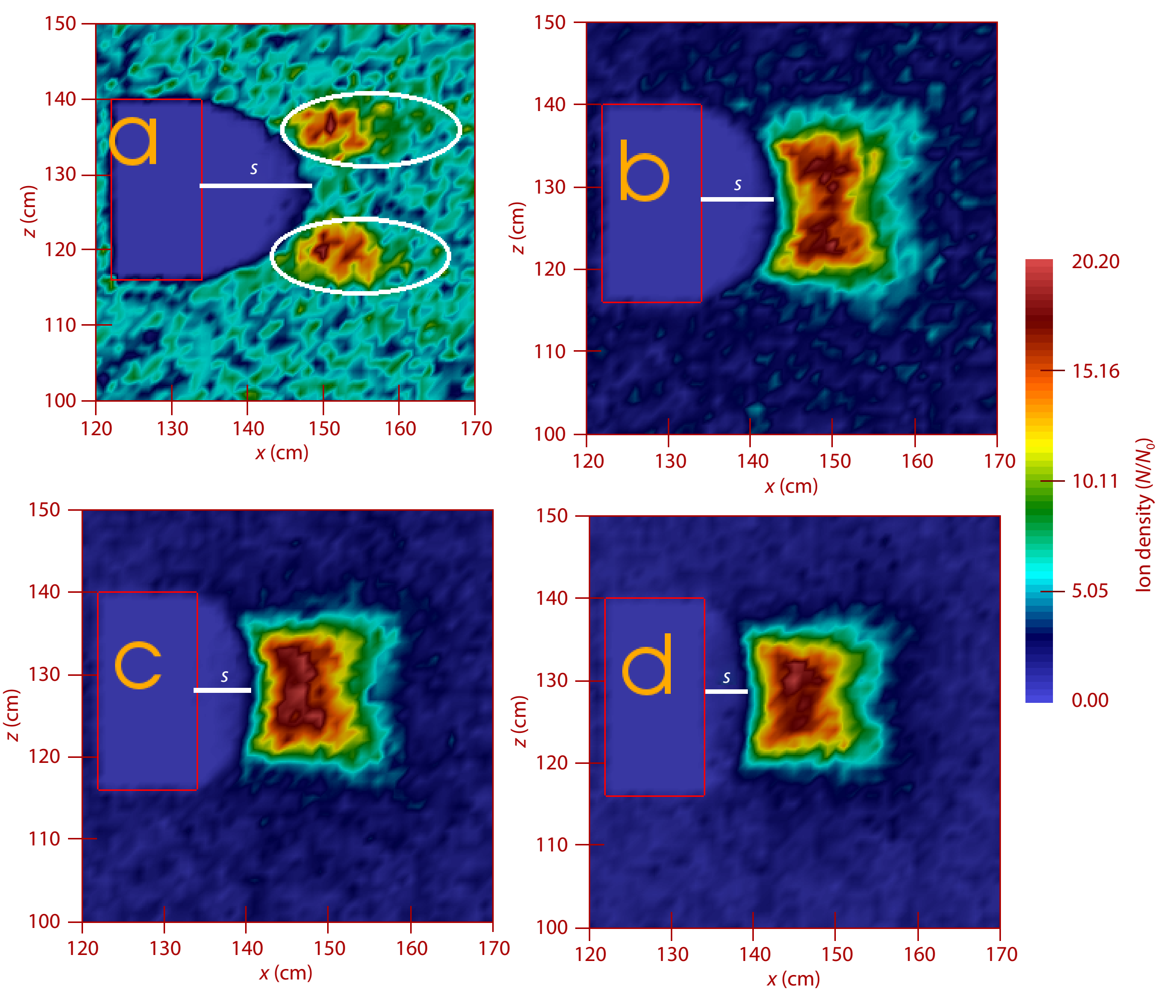

Figure 2. Ion-focusing configuration in the downstream area for case 1 in the *x*–*z* plane with fixed potentials of −5 V (a), −10 V (b), −15 V (c), and −20 V (d). Only a cross section of the simulation box is shown. The two white ellipses indicate the presence of the two-ion streamers at the sheath edges of the spacecraft.

ion void structure, denoted by the white *s*, diminishes with a decrease in the object potential.

In the simulation, the use of a rectangular body to represent the spacecraft geometry leads to different ion deflection behaviors along the *z* and *y* directions. This geometric asymmetry can explain certain features observed in Figure 2. Most notably, the two-ion density peaks at the upper and lower edges of the body result from a combination of deflections in both the *z* and *y* directions. On the other hand, a relatively reduced ion density can be seen in the area between these peaks, where *y*-direction deflection predominates. Similar dual-peak patterns are also visible in the other panels, but with reduced concentrations. Although they are less visible, similar dual-peak features can also be seen in the other panels in Figure 2.

Furthermore, we investigate ion-focusing formation in the downstream region at a potential of −5 V for cases 1 to 3, as illustrated in Figure 3. At a constant potential, a decrease in T_r diminishes the ion-focusing region, ultimately revealing the original ion void structure. Note that the flows of plasma are not totally absorbed by the spacecraft because of the negative potential. The flows of plasma at the upper and lower edges of the spacecraft are deflected toward the wake field. As shown in Figure 3, the ion concentration starts dispersing in cases 2 and 3 and conjoins, fulfilling the near-wake region shown in case 1. Thus, we can infer that increasing T_r drives the ion concentration to become more compact and more focused in a certain region, leading to a two-ion streamer whose evolution can clearly be seen through cases 2 and 3.

In all instances, the ion void zone, characterized by a negative potential and a much larger electron density than ion density, progressively vanishes and transforms into an ion-rich or ion-focusing region. A higher magnitude of negative potential generates more ion aggregation, creating an ion focus behind the item, as shown in Figure 2. Moreover, an increased temperature ratio results in a greater concentration of ions, as shown by the two-ion streamer (white ellipses) in Figure 3. The distortions of the ion void structure shown in Figure 2 range from approximately $2\lambda_D$ (upper left) to approximately $1.5\lambda_D$ (upper right), $0.9\lambda_D$ (lower left), and $0.5\lambda_D$ (lower right).

This study defines local ion focusing as the configuration of a two-ion streamer originating at the upper and lower edges of the rear of the spacecraft, as illustrated in Figure 2a (white ellipses). Conversely, ion focusing pertains to the amalgamation of these two-ion streamers, as depicted in Figures 2b, 2c, and 2d. As shown in Figure 3, when the object potential is uniform, the local ion focusing manifests as two streamers that are mostly determined by the temperature ratio. The temperature ratio is relevant to producing two-ion streamers rather than the ion-focusing formation. The pronounced reliance of ion focusing on the object potential is clearly shown by the signature described previously in Figures 2b, 2c, and 2d, whereby a reduction in the object potential (negative) may draw in more ions and expedite their movement to occupy the original ion void area. Nonetheless, we must further investigate the reliance of ion focusing on the temperature ratio, T_r, along with other characteristics discussed in the subsequent section.

3.2 Fixed Potential with Constant Parameters

We conduct further simulations to investigate the parameters that predominantly influence the ion-focusing formation. For these simulations, the following parameters are established: (1) the electron temperature (T_e) is altered while the other parameters are held constant (case 4); (2) only the ion temperature (T_i) is allowed to exhibit fluctuations (case 5); (3) only the ambient plasma density (N_p) is altered (case 6); and (4) only the auroral electron density (N_{ae}) is allowed to be subject to variation (case 7).

Table 1 presents the configuration of each case. Here, we set one parameter to change and the others to remain constant to identify which parameter prominently drives the ion-focusing formation. The results of the simulations show that, overall, the parameters used in cases 4 to 7 play a role only in two-ion streamer formation, resembling the structures in cases 1 and 2, as shown in Figure 3.

In case 4, when the electron temperature changes are set across the case, we cannot see its contribution to modifying the focusing structure. The ion-focusing structure in each subcase shows a pattern similar to Figure 3 (middle panel), and no distortion occurs. We initially presumed that the higher the electron temperature, the more ions would be focused on the downstream side, as shown in the previous simulation, but case 4 does not show this feature. It is also obvious that the temperature ratio (T_r) increases over the subcase in case 4. Thus, the variability of T_r does

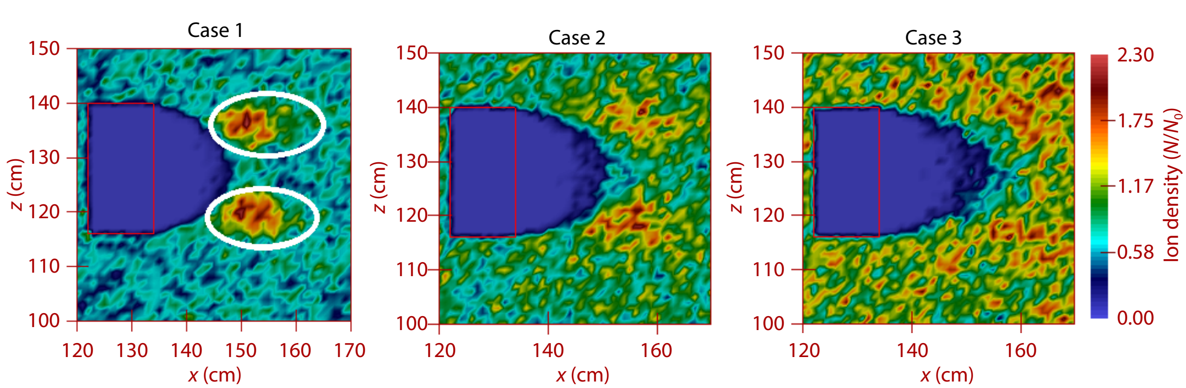

Figure 3. The formation of an ion-focusing region on the downstream side of the spacecraft at the constant potential of −5 V for $T_r = 5$ (case 1), $T_r = 2$ (case 2), and $T_r = 1.1$ (case 3).

not significantly contribute to ion-focusing formation but rather to a two-ion streamer.

Additionally, we analyze case 5, in which the ion temperature varies throughout the case while other parameters remain unchanged. The simulation results exhibit a structure analogous to case 2 in Figure 3. The effects of ion temperature variations (T_i) and the temperature ratio (T_r) on the modified ion-focusing structure are not evident. An effective indicator of this feature is observed in the two separated ion structures depicted in case 2 of Figure 3, which do not merge to form an integrated structure, but instead remained detached at the upper and lower edges of the rear object. Local changes in the two-ion streamer structure are observed in each subcase; however, these changes are minimal and can be disregarded.

Subsequently, we conduct a simulation for case 6 with the parameters outlined in Table 1, resulting in a structure comparable to case 2 in Figure 3. The ambient plasma density diminishes in the subcase outlined in Table 1. Increasing the ambient density (subcase a) results in concentrated ions at both edges, similar to the structure observed in case 1 of Figure 3. The ion density is observed to concentrate and become more compact at both edges. Consequently, an increase in ambient plasma density, corresponding to a decrease in the density ratio of auroral electrons to ambient plasma, results in a more pronounced two-ion streamer structure behind the object. The variation in ambient plasma density near the spacecraft contributes to the formation of local ion focusing, manifesting as a two-ion streamer.

We also investigate how much the density ratio of auroral electrons to ambient plasma density will influence ion focusing, as demonstrated in case 7 from Table 1. We identify a characteristic comparable to case 2 in Figure 3. The variation in auroral electron density makes a nonsignificant contribution to the enhancement of ion density in the downstream region. The characteristics of all cases exhibit similarity in that the two distinct ion concentration regions do not extend toward the wake centerline, maintaining a relatively stable structure. Nevertheless, the simulation conducted in case 7 highlights that the density ratio has a negligible impact on the formation of ion focusing.

The interaction between the spacecraft and ambient plasma, along with precipitating auroral electrons in the LEO environment, is complex because of their highly non-Maxwellian distribution (Harris, 2003). In most instances, the Maxwell distribution is selected as a fundamental assumption for practical applications. In the case of a spacecraft subjected to a very low potential concerning the surrounding plasma, a wake is generated, forming an ion void region resulting from mesosonic motion. This effect occurs because the motion of the spacecraft exceeds the thermal motion of ions, resulting in a delay for ions to populate the ion void in the wake field. Under specific conditions, the ion void region characterized by a negative potential may be distorted, particularly when the spacecraft potential decreases significantly.

The physics of ion focusing is thoroughly elucidated here. It pertains to the ambient polar electric field resulting from pressure or density gradients in the wake zone. Figure 4 illustrates the creation of an ion-focusing structure in the z direction. Note that the deflection of ion flow also occurs in the y direction. Because of the smaller dimension of the body in the y-axis, it is difficult to see the ion deflection structure in that direction. However, deflection in the y direction also plays an important role in ion deflection in addition to the z direction. As shown in Figure 4, flowing plasma through a solid object can be seen to induce ion compression on the ram side (anterior to the spacecraft body). Ions will be guided and accelerated by an electric field generated by the supersonic movement of the object. The ion density escalates on this side, whereas the electron density diminishes, forming a sheath. The decrease in the density ratio of ions to electrons on the ram side indicates the presence of the sheath area. The influence of mesosonic motion creates an ion vacuum zone downstream. Unlike the upstream zone, electrons mostly scatter, resulting in a negative potential inside the ion-empty region.

At the sheath edges of the body (upper and lower), the ion trajectories passing through these narrow regions begin to be deflected by the local electric field at the sheath edges. As the ions persistently traverse the electric field while moving into the downstream region, their paths will converge along or about the wake centerline, resulting in a zone of elevated ion concentration

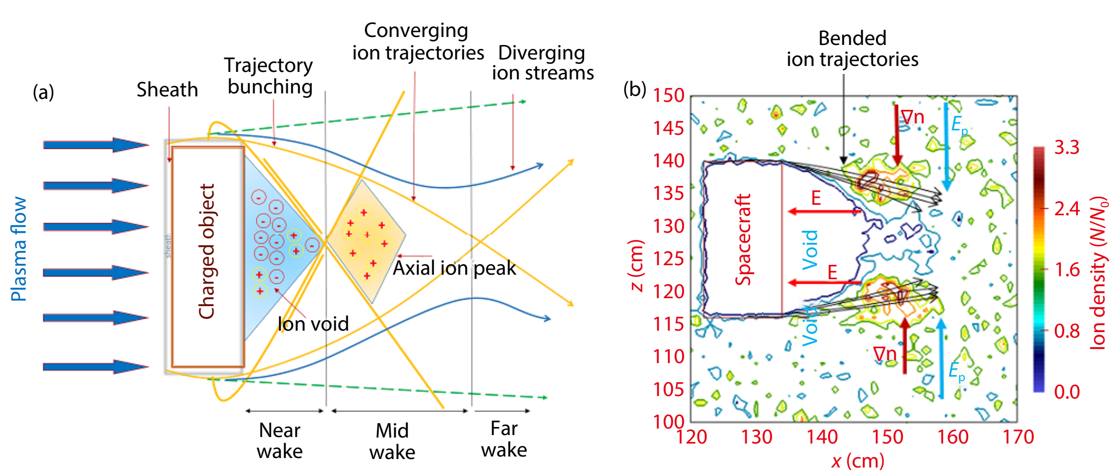

Figure 4. The formation of an ion-focusing structure in the downstream region of the spacecraft: (a) schematic diagram based on Stone (1981); (b) the proposed mechanism for the two-ion streamer and ion-focusing formation in the present study.

(ion focusing). Additionally, because of this concentration, ion repopulation in the wake field may occur. The negative space potential inside the ion void area causes repopulated ions to move toward the object, with the migration rate dependent on the potential. A density gradient is present in the downstream zone, as shown by all the examples in our investigation. The immediate process of ion focusing involves two distinct ion structures in our work, as shown in Figure 4b.

Figure 4b illustrates the clustering of ion paths inside the wake field. The electric field at the sheath edges deflects the ion trajectories. A density gradient (n) formation in the wake field results in plasma expansion, whereby ions are accelerated and then guided by the ambipolar electric field (E_p) toward the wake centerline. In the absence of ion deflection, theoretically an ion density rarefaction extends into the downstream zone, with its angle (θ) being proportional to the Mach number (M). As the angle θ lowers, the ion density rises (Wang J and Hastings, 1992), resulting in a higher ion density in the wake zone across all instances in the present investigation. Nevertheless, the rarefaction of ion density is contravened, resulting in two ion-rich forms. As shown in Figure 4b, the convergence of ion paths from both edges does not occur, resulting in two distinct structures.

As the amplitude of the spacecraft potential increases, the contribution to an ion-focusing formation comes from the ambipolar electric field generated by plasma expansion in the wake field and the electric field induced by the spacecraft itself (E). The electric field intensifies as the potential diminishes. While facilitating ion focusing by trajectory deflection, the ensuing electric field also draws the deflected ions toward the spacecraft, reducing the ion void structure. This process elucidates the radial inward expansion of the ion-focusing structure, as shown in Figure 2, as the potential of the object becomes more negative.

Simulations conducted by establishing a stable potential on the spacecraft and allowing a specific parameter to vary demonstrated that variations in T_e and T_i (cases 4 and 5) and N_{ae} (case 7) contribute little to the creation of ion focusing. The fluctuation of ambient plasma density around the item can alter the local ion-focusing configuration, resulting in a two-ion streamer. The density ratio of auroral electrons to ambient plasma in example 7 fluctuates, similar to case 6, although it does not influence the ion-focusing structures because of the static ambient density.

Moreover, we observed no significant correlation between variation of the temperature ratio and the ion-focusing formation. We should point out that we refer to the term “ion focusing” as the ion-rich region as part of the repopulated ions that distort the ion void structure in the wake region. Thus, it occurs when two-ion streamers at the upper and lower edges of the spacecraft incorporate and migrate toward the spacecraft. Instead, the two-ion streamers at the upper and lower edges of an object are referred to as “local ion focusing.”

The relationship between ion-focusing production and the temperature ratio remains ambiguous in this investigation. This result sharply contradicts the work of Miloch (2010), which indicated that ion focusing is temperature dependent. We recognize that variations in temperature ratio influence only the local ion-focusing structure as a result of the electric field effects from the sheath edges of the object, with plasma expansion resulting from the density gradient in the downstream area. The sole parameter influencing ion focusing is the potential variation, wherein a more negative object potential, resulting from the electric field produced by the spacecraft potential and the ambipolar electric field generated by plasma expansion, will accelerate and direct ions into the ion void region, leading to the repopulation of ions in the wake field. This trait is well depicted in Figure 2.

4. Conclusions

Numerous simulations were conducted to identify the parameter that predominantly influences ion-focusing formation in the wake region. This study defines ion focusing as an ion-dense area where multiple ions migrate to replenish the wake field and distortion void structures. Consequently, the ion density rapidly increases and modifies the space potential. In most cases in this study, a large-magnitude spacecraft potential repels electrons omnidirectionally, whereas the electric field accelerates ions inside the sheath in the upstream region. The ion repopulation process gradually distorts the initial ion void region on the downstream side.

The repopulation of ions in the wake region is linked to ion trajectory deflection as they pass through the sheath edges of the spacecraft. The electric field effectively bends these trajectories, as indicated by the formation of two-ion streamers further downstream. Because of the density gradient that creates ambipolar electric fields, ions are accelerated toward the wake centerline. When the convergence of ion trajectories from both edges does not take place, the two-ion streamers remain distinct in a vicinity around the wake centerline. As the potential becomes more negative, the generated electric field and the ambipolar electric field accelerate a bunch of ion streamers toward the spacecraft, leading to ion void distortion. With a very high negative potential, the ion void area can vanish and transform into an ion-focusing region. In most cases in the present study, the fixed negative potentials are not so large, and we can see the ion void structure despite ion focusing in the wake field.

The further investigation of various environmental parameters resulted in discrepancies in the temperature ratio. The dependence of the temperature ratio on ion-focusing formation is not clear in the present study. It facilitates only local ion focusing as a two-ion streamer, characterized by a strong concentration at the upper and lower margins, which then disperses farther downstream. Nonetheless, potential fluctuation is the only characteristic significantly influencing ion-focusing formation in the downstream area. Thus, in the case of fixed potentials, the contribution of the geophysical parameters presented in this study to ion-focusing formation is nonsignificant except for the object potential itself. Consequently, it transpires when two-ion streamers at the upper and lower peripheries of the spacecraft converge and advance toward the spacecraft.

Acknowledgments

The main author would like to thank Kobe University and the National Research and Innovation Agency (BRIN) for providing facilities and other support for this research. The material for the present paper was produced during a Ph. D. course at Kobe University, and the BRIN Smart Mechatronics Research Group, which was partially funded by Telkom University, continued this research analysis. Finally, the authors thank NASA for providing valuable research data.

The authors declare that there is no conflict of interest regarding the publication of this article. The authors confirm that the paper is free of plagiarism.

References

Ahmad, N., Herdiwijaya, D., Djamaluddin, T., Usui, H., and Miyake, Y. (2018a). Diagnosing low earth orbit satellite anomalies using NOAA-15 electron data associated with geomagnetic perturbations. *Earth Planets Space*, *70*(1), 91. https://doi.org/10.1186/s40623-018-0852-2

Ahmad, N., Usui, H., and Miyake, Y. (2018b). Particle in cell simulation to study the charging and evolution of wake structure of LEO spacecraft. In *18th Asia Simulation Conference on Methods and Applications for Modeling and Simulation of Complex Systems* (pp. 255–268). Kyoto, Japan: Springer. https://doi.org/10.1007/978-981-13-2853-4_20

Ahmad, N., Usui, H., and Miyake, Y. (2019). The Particle-In-Cell simulation on LEO spacecraft charging and the wake structure using EMSES. *J. Adv. Simul. Sci. Eng.*, *6*(1), 21–31. https://doi.org/10.15748/jasse.6.21

Ahmad, N., and Usui, H. (2020). Numerical simulation of spacecraft charging attributed to ionospheric plasma in polar and equatorial environment. *Indones. J. Geogr.*, *52*(1), 98–104. https://doi.org/10.22146/ijg.50564

Baumjohann, W., and Treumann, R. A. (1997). *Basic Space Plasma Physics*. London: Imperial College Press.

Endo, K., Kumamoto, A., and Katoh, Y. (2015). Observation of wake-induced plasma waves around an ionospheric sounding rocket. *J. Geophys. Res.: Space Phys.*, *120*(6), 5160–5175. https://doi.org/10.1002/2014JA020047

Engwall, E., Eriksson, A. I., and Forest, J. (2006). Wake formation behind positively charged spacecraft in flowing tenuous plasmas. *Phys. Plasmas*, *13*(6), 062904. https://doi.org/10.1063/1.2199207

Frooninckx, T. B., and Sojka, J. J. (1992). Solar cycle dependence of spacecraft charging in low Earth orbit. *J. Geophys. Res.: Space Phys.*, *97*(A3), 2985–2996. https://doi.org/10.1029/91ja02704

Garrett, H. B., and Whittlesey, A. C. (2000). Spacecraft charging, an update. *IEEE Trans. Plasma Sci.*, *28*(6), 2017–2028. https://doi.org/10.1109/27.902229

Harris, J. T. (2003). Spacecraft charging at geosynchronous altitudes: current-balance and critical temperature in a non-maxwellian plasma. Wright-Patterson Air Force Base, Ohio, USA: Air Force Institute of Technology.

Hastings, D., and Garrett, H. (1996). *Spacecraft–Environment Interactions*. Cambridge: Cambridge University Press. https://doi.org/10.1017/CBO9780511525032

Hastings, D. E. (1995). A review of plasma interactions with spacecraft in low Earth orbit. *J. Geophys. Res.: Space Phys.*, *100*(A8), 14457–14483. https://doi.org/10.1029/94ja03358

Katz, I., Mandell, M., Parks, D., Wright, K., Stone, N., and Samir, U. (1986). The Effect of Object Potentials on the Wake of a Flowing Plasma. Scientific report No.3, Hanscom Air Force Base, Massachusetts, USA.

Katz, I., Mandell, M. J., Parks, D. E., Wright, K., Stone, N. H., and Samir, U. (1987). Effect of object potentials on the wake of a flowing plasma. *J. Appl. Phys.*, *62*(7), 2675–2679. https://doi.org/10.1063/1.339418

Koons, H. C., Mazur, J. E., Selesnick, R. S., Blake, J. B., Fennell, J. F., Roeder, J. L., and Anderson, P. C. (2000). The impact of the space environment on space systems. In *6th Spacecraft Charging Technology Conference* (pp. 7–11), AFRL Science Center, Hanscom AFB, MA, USA.

Miloch, W. J. (2010). Wake effects and Mach cones behind objects. *Plasma Phys. Control. Fusion*, *52*(12), 124004. https://doi.org/10.1088/0741-3335/52/12/124004

Miyake, Y., and Usui, H. (2009). New electromagnetic particle simulation code for the analysis of spacecraft–plasma interactions. *Phys. Plasmas*, *16*(6), 062904. https://doi.org/10.1063/1.3147922

Okada, M., Omura, Y., and Matsumoto, H. (1995). Computer experiments of spacecraft–plasma interactions in a dilute and high-β_e plasma with a fast plasma flow. *J. Geophys. Res.: Space Phys.*, *100*(A11), 21549–21559. https://doi.org/10.1029/95ja01525

Stone, N. H. (1981). The aerodynamics of bodies in a rarefied ionized gas with applications to spacecraft environmental dynamics. *NASA Tech. Pap.*, 1933. https://ntrs.nasa.gov/api/citations/19820007243/downloads/19820007243.pdf

Wang, J., and Hastings, D. E. (1992). Ionospheric plasma flow over large high-voltage space platforms. II: The formation and structure of plasma wake. *Phys. Fluids B: Plasma Phys.*, *4*(6), 1615–1629. https://doi.org/10.1063/1.860070